Arabian Journal of Chemistry (2020) **13**, 3903–3909

King Saud University

Arabian Journal of Chemistry

www.ksu.edu.sa
www.sciencedirect.com

ORIGINAL ARTICLE

Synthesis, characterization, antibacterial studies and quantum-chemical investigation of the new fluorescent Cr(III) complexes

Shohreh Rastegarnia, Mehdi Pordel *, Sadegh Allameh

Department of Chemistry, Mashhad Branch, Islamic Azad University, Mashhad, Iran

Received 2 January 2019; accepted 5 March 2019
Available online 13 March 2019

KEYWORDS

Benzimidazole;
Cr(III) complex;
UV–Vis and fluorescence spectroscopy;
DFT;
Antibacterial activity

Abstract Coordination of the ligands derived from benzimidazole with Cr(III) led to the formation of new fluorescent Cr (III) complexes. The structures of the new complexes were established by spectral, analytical data and Job's method and an octahedral geometry was proposed for the complexes. Also, the DFT methods were employed to gain a deeper insight into geometry and spectral properties of the new Cr (III) complexes. The DFT-calculated vibrational modes of Cr(III) complexes are in good agreement with the experimental values, confirming suitability of the optimized geometries for the complexes. Fluorescent ligands and chromium complexes were spectrally characterized by UV–Vis and fluorescence spectroscopy. Results revealed that Cr(III) complexes generate fluorescence in dilute solution of DMSO. Calculated electronic absorption spectra were also provided by time-dependent density functional theory (TD-DFT) method. The new complexes exhibited potent antibacterial activity against a panel of strains of Gram negative bacterial and Gram positive species and their MIC was also determined. Two strains of Gram positive and two strains of Gram negative bacteria.

1. Introduction

The search for new antibacterial compounds continues to be very active because the resistance to the antibacterial agents is nowadays recognized as a major global public health problem.

The Cr chemicals play an important role in several industrial processes such as leather tanning, mining of chrome ore, production of steel and alloys, dyes and pigment manufacturing, glass industry, wood preservation, textile industry, film and photography, metal cleaning, plating and electroplating, etc. (Sarin et al., 2006). Chromium (III) is a significant bioelement responsible for many catalytic processes in living systems (Mandina and Tawanda, 2013). It is present in the active centers of many enzymes, which is why it is classified as one of the essential elements. It facilitates the transport of glucose from the blood to the cells (Chen et al., 2009) and cooperates

* Corresponding author.
E-mail address: mehdipordel58@mshdiau.ac.ir (M. Pordel).
Peer review under responsibility of King Saud University.

Production and hosting by Elsevier

https://doi.org/10.1016/j.arabjc.2019.03.001
1878-5352

with insulin in protein synthesis (Ziegenfuss et al., 2017). Cr (III) has been shown to have a detrimental effect on various components of the immune system, giving rise to immune stimulation or immune inhibition (Adam et al., 2017). Chromium (III) also plays an important function in lipid metabolism thus reducing the risk of atherogenesis (Chen et al., 2017), increase in lean body mass (Liu et al., 2015), and promotion of weight loss (Whitfield et al., 2016). Chromium(III) chelates have been found to interact with biological systems and to exhibit antineoplastic activity (Abdel-Rahman et al., 2017) and antibacterial, antifungal (Ghssein and Matar, 2018; El-Megharbel and Refat, 2015), and anticancer activity (Mahmoud et al., 2015). Some chromium (III) N,S,O/N,N-donor chelators are good anticancer agents due to strong binding ability with DNA base pair (Zhou et al., 2016).

On the other hand, benzimidazole nucleus is one of the most important heterocycles in medicinal chemistry. Owing to the great structural diversity of biologically active benzimidazole, it is not surprising that the benzimidazole nucleus has become a significant structural component in many pharmaceutical agents. Benzimidazole can be found in a wide range of bioactive compounds such as antiparasitics (Flores-Carrillo et al., 2017), anticonvulsants (Siddiqui et al., 2016), analgesics (Siddiqui et al., 2016), antihistaminics (Ding et al., 2017), antiulcers (Saini et al., 2016), antihypertensives (Zhang et al., 2015), antiviral (Vausselin et al., 2016), anticancers (Kumar et al., 2016), antifungals (Keller et al., 2015), anti-inflammatory agents (Gaba et al., 2014), proton pump inhibitors (Van Oosten et al., 2017) and anticoagulants (Yang et al., 2016). Optimization of substituents around the benzimidazole nucleus has resulted in many drugs like albendazole, mebendazole, thiabendazole as antihelmintics; omeprazole, lansoprazole, pantoprazole as proton pump inhibitors; astemizole as antihistaminic; enviradine as antiviral; candesarten cilexitil and telmisartan as antihypertensives and many lead compounds in a wide range of other therapeutic areas. Also, benzimidazoles play an important role in determining the function of a number of biologically important metal complexes (Bansal and Silakari, 2012).

Since, chromium and benzimidazole play a key role in biological systems, it is important to study the interactions of benzimidazole ligands with chromium. This paper describes the synthesis, spectral and density functional theory (DFT) calculations of three new chromium (III) complexes of fluorescent heterocyclic ligands derived from benzimidazole. Antibacterial activities of the compounds against Gram-positive and Gram-negative bacterial species were also determined.

2. Experimental

2.1. Equipment and materials

Percentage of the Cr(III) was measured by using a Hitachi 2-2000 atomic absorption spectrophotometer. The ^{13}C NMR (75 MHz) and ^{1}H NMR (300 MHz) spectra were obtained on a Bruker Avance DRX-300 spectrometer. Chemical shifts are reported in ppm downfield from TMS as internal standard; coupling constant J is given in Hz. The FT-IR spectra were recorded as potassium bromide pellets using a Tensor 27 spectrometer and only noteworthy absorptions are listed. The mass spectrum was recorded on a Varian Mat, CH-7 at 70 eV and ESI mass spectrum was measured using a Waters Micromass ZQ spectrometer. Elemental analysis was performed on a Thermo Finnigan Flash EA microanalyzer. Absorption and fluorescence spectra were recorded on Varian 50-bio UV–Visible spectrophotometer and Varian Cary Eclipse spectrofluorophotometer. UV–Vis and fluorescence scans were recorded from 200 to 1000 nm. Melting points were obtained on an Electrothermaltype-9100 melting-point apparatus.

The microorganisms *Bacillus subtilis* ATCC 6633, *Pseudomonas aeruginosa* ATCC 27853 and *Escherichia coli* ATCC 25922 were purchased from Pasteur Institute of Iran and *Methicillin Resistant S. aureus (MRSA)* was isolated from different specimens which were referred to the Microbiological Laboratory of Ghaem Hospital of Medical University of Mashhad, Iran and its methicillin resistance was tested according to the NCCLS guidelines.

All solvents were dried according to standard procedures. Compounds **1** (Preston, 1990) and **3a,c** (Rahimizadeh et al., 2009) were obtained according to the published methods. Other reagents were commercially available.

2.2. Computational methods

All of the calculations have been performed using the DFT method with the B3LYP functional (Lee et al., 1988) as implemented in the Gaussian 03 program package (Frisch and Et, 2003). The 6-311 + + G(d, p) basis sets were employed except for the Cr(III) where the LANL2DZ basis sets were used with considering its effective core potential. Geometry of the Cr(III) complexes was fully optimized, which was confirmed to have no imaginary frequency of the Hessian. Geometry optimization and frequency calculation simulate the properties in the gas/solution phases.

The fully-optimized geometries were confirmed to have no imaginary frequency of the Hessian.

The solute-solvent interactions have been investigated using one of the self-consistent reaction field methods, i.e., the Polarizable Continuum Model (PCM) (Tomasi and Cammi, 1995).

2.2.1. General procedure for the synthesis of ligands *4a-c* from *3a-c*

To a solution of **3a**-c (6 mmol) in EtOH (40 mL) and HCl (2 M, 3 mL), iron powder (0.89 g, 16 mmol) was added with stirring. Then, the mixture was refluxed for 4 h and then poured into water. The precipitate was collected by filtration, washed with water, and air-dried to give crude **4a**-c.

(5-Amino-1-ethyl-1H-benzo[d]imidazol-4-yl)(phenyl)methanone (**4a, L1**) was obtained as a shiny yellow needles (EtOH). mp.: 186–188 °C [Lit mp. 185–187 °C] (Rahimizadeh et al., 2009); ^{1}H NMR ($CDCl_3$): δ 1.51 (t, J = 7.5 Hz, 3H, CH_3), 3.89 (br s, 2H, NH_2), 4.13 (q, J = 7.5 Hz, 2H, NCH_2), 6.67 (d, J = 8.5 Hz, 1H, Ar H), 7.09 (d, J = 8.5 Hz, 1H, Ar H), 7.20–7.49 (m, 5H, Ar H), 7.78 (s, 1H, Ar H) ppm; ^{13}C NMR ($CDCl_3$): δ 14.1, 41.9, 111.0, 114.2, 114.7, 125.3, 127.2, 127.6, 127.6, 129.2, 132.1, 135.8, 142.0, 195.7 (C═O) ppm. IR (KBr): 3317, 3260 cm^{-1} (NH_2), 1633 cm^{-1} (C═O). MS (m/z) 279 (M^+). Anal. Calcd for $C_{16}H_{15}N_3O$ (265.3): C, 72.43; H, 5.70; N, 15.84. Found: C, 72.66; H, 5.73; N, 16.03.

(5-Amino-1-propyl-1H-benzo[d]imidazol-4-yl)(phenyl)methanone (**4b, L2**) was obtained as a shiny yellow needles (EtOH). mp.: 122–124 °C [Lit mp. 121–123 °C] (Rahimizadeh

et al., 2009); ^{1}H NMR ($CDCl_3$): δ 0.94 (t, J = 7.5 Hz, 3H, CH_3), 1.75–2.10 (m, 2H, CH_2), 4.04 (t, J = 7.5 Hz, 2H, NCH_2), 4.12 (br s, 2H, NH_2), 6.62 (d, J = 8.5 Hz, 1H, Ar H), 7.03 (d, J = 8.5 Hz, 1H, Ar H), 7.11–7.52 (m, 5H, Ar H), 7.75 (s, 1H, Ar H) ppm; ^{13}C NMR ($CDCl_3$): δ 11.4, 23.2, 46.8, 111.3, 114.1, 114.8, 125.5, 127.1, 127.6, 127.9, 129.0, 132.3, 135.6, 142.2, 195.9 (C═O) ppm. IR (KBr): 3315, 3260 cm^{-1} (NH_2), 1635 cm^{-1} (C═O). MS (m/z) 279 (M^+). Anal. Calcd for $C_{17}H_{17}N_3O$ (279.3): C, 73.10; H, 6.13; N, 15.04. Found: C, 73.45; H, 6.15; N, 14.87.

*(5-Amino-1-butyl-1H-benzo[d]imidazol-4-yl)(phenyl)methanone (**4c, L3**)* was obtained as a shiny yellow needles. m.p.: 117–119 °C. Yield: 79%. ^{1}H NMR ($CDCl_3$): δ 0.89 (t, J = 7.5 Hz, 3H, CH_3), 1.21–1.33 (m, 2H, CH_2), 1.77–1.88 (m, 2H, CH_2), 4.19 (br s, 2H, NH_2), 4.31 (t, J = 6.9 Hz, 2H, NCH_2), 6.67 (d, J = 8.5 Hz, 1H, Ar H), 7.01 (d, J = 8.5 Hz, 1H, Ar H), 7.09–7.47 (m, 5H, Ar H), 7.73 (s, 1H, Ar H) ppm; ^{13}C NMR ($CDCl_3$): δ 13.7, 20.01, 33.1, 44.5, 110.8, 114.3, 114.6, 125.3, 127.1, 127.4, 127.8, 128.8, 132.5, 135.9, 142.0, 195.3 (C═O) ppm. IR (KBr): 3320, 3263 cm^{-1} (NH_2), 1637 cm^{-1} (C═O). MS (m/z) 293 (M^+). Anal. Calcd for $C_{18}H_{19}N_3O$ (293.4): C, 73.69; H, 6.53; N, 14.32. Found: C, 74.01; H, 6.57; N, 14.09.

2.2.2. General procedure for the synthesis of the complexes *5a-c* from ligands *4a-c*

Chromium(III) nitrate nonahydrate (0.25 gr, 1 mmol) was added to the yellow solution of ligand **4a-c** (2 mmol) in aqueous metanolic solution (15 mL, MeOH, H_2O, 10:90), resulting in color change to orange. The reaction was carried out for another 1 h at rt. The complex was isolated by evaporation of the solvent and washed with cold MeOH and then H_2O.

$[Cr(L1)_2]N_3O_9{\cdot}2(H_2O)$ (**5a**): was obtained as an orange powder. mp. > 300 °C (decomp). IR (KBr): 3389, 3250 cm^{-1} (NH_2), 1628 cm^{-1} (C═O), ESI-MS (+) m/z (%): 582 $[Cr(L1)_2]^{3+}$. Anal. Calcd for $C_{32}H_{34}CrN_9O_{13}$ (804.2): C, 47.76; H, 4.26; N, 15.67; Cr, 6.46. Found: C, 47.93; H, 4.29; N, 15.83; Cr, 6.59.

$[Cr(L2)_2]N_3O_9{\cdot}2(H_2O)$ (**5b**): was obtained as an orange powder. mp. > 300 °C (decomp). IR (KBr): 3363, 3257 cm^{-1} (NH_2), 1629 cm^{-1} (C═O), ESI-MS (+) m/z (%): 610 $[Cr(L2)_2]^{3+}$. Anal. Calcd for $C_{34}H_{38}CrN_9O_{13}$ (832.2): C, 49.04; H, 4.60; N, 15.14; Cr, 6.24. Found: C, 49.28; H, 4.64; N, 15.29; Cr, 6.39.

$[Cr(L3)_2]N_3O_9{\cdot}2(H_2O)$ (**5c**): was obtained as an orange powder. mp. > 300 °C (decomp). IR (KBr): 3371, 3260 cm^{-1} (NH_2), 1625 cm^{-1} (C═O), ESI-MS (+) m/z (%): 638 $[Cr(L3)_2]^{3+}$. Anal. Calcd for $C_{36}H_{42}CrN_9O_{13}$ (860.2): C, 50.23; H, 4.92; N, 14.65; Cr, 6.04. Found: C, 49.80; H, 4.89; N, 14.51; Cr, 6.31.

3. Results and discussion

3.1. Synthesis and structure of the new ligands *4a-c* and complexes *5a-c*

5-Nitro-1*H*-benzimidazole was alkylated with different alkyl halides in KOH and DMF according to the literature method (Preston, 1990). Reaction of compounds **1a-c** with benzyl cyanide (**2**) in basic MeOH solution led to the formation of 3-alkyl-8-phenyl-3*H*-imidazo[4′,5′:3,4]benzo[1,2–c]isoxazole (**3a-c**) (Rahimizadeh et al., 2009). Aryl ketons **4a-c** were obtained by reduction of compounds **3a-c** in EtOH by Fe/HCl in high yields (Scheme 1).

^{1}H, ^{13}C NMR, FT-IR spectra and analytical data proved the structure of the compounds **4a-c**. For example, in the ^{1}H NMR spectrum of compound **4c** there is an exchangeable peak at δ 4.19 ppm attributed to NH_2 group protons. Also, there are two doublet signals (δ = 6.67 and 7.01 ppm), a multiplet signal (δ = 7.09–747 ppm) and singlet signal (δ = 7.73 ppm) assignable to eight aromatic rings protons. In addition, 16 different carbon atom signals are observed in the ^{13}C NMR spectrum of compound **4c**. In addition, the FT-IR spectrum of compound **4c** in KBr revealed a broad absorption bands at 3320 and 3263 cm^{-1} attributed to NH_2 and 1637 cm^{-1} assignable to the C═O groups. Also, the results of mass spectroscopy (m/z 293 $[M]^+$) and elemental analyses support the structure of the compound **4c**.

The new complexes **5a-c** were obtained from reaction of ligands **4a-c** and $Cr(NO_3)_3{\cdot}9H_2O$ in 2:1 M ratio obtained by Job's method (Fig. 1) (Vosburgh and Chromium, 1941) in aqueous metanolic solution. For example, the Job's plot reached a maximum value at a mole fraction of 0.33, which confirmed that molar ratio between Cr(III) ions and **4a** in the complex **5a** is 1:2.

The structural assignments of the new complexes **5a-c** were based on the elemental and spectroscopic (IR, and mass) analyses. The elemental analysis results for Cr complexes confirm the proposed $[Cr(L)_2]N_3O_9{\cdot}2(H_2O)$ formula. In addition, molecular ion peak at m/z 582 ($[Cr(L1)_2]^{3+}$), m/z 610 ($[Cr(L2)_2]^{3+}$) and m/z 638 ($[Cr(L3)_2]^{3+}$) strongly support the structure of the new complexes **5a, 5b** and **5c** respectively.

An octahedral geometry was proposed for Cr(III) complexes **(5a-c)** based on our experimental results and reported literatures (Yousefi et al., 2015; Liu et al., 2015) (see Scheme 2).

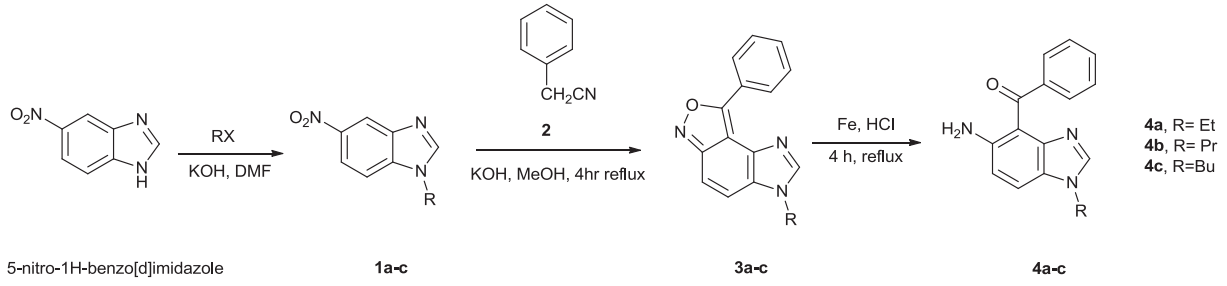

Scheme 1 Synthesis of the ligands **4a-c.**

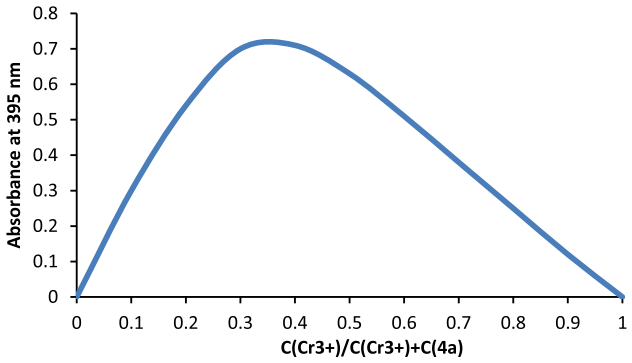

Fig. 1 Job's curve of equimolar solutions for complex **5a** in aqueous methanolic solution.

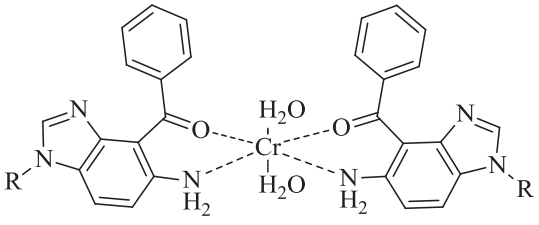

5a, R=Et
5b, R=Pr
5c, R=Bu

Scheme 2 The structure of the new Cr(III) complexes **5a-c**.

The calculated data could help to gain a deeper insight into geometry and spectral properties of the new Cr (III) complexes. Therefore, geometry of Cr(III) complex (**5a**) were optimized in both of the gas phase and MeOH as the solvent (PCM model) by DFT calculations at the B3LYP/6–311 + + G(d,p) level. The optimized geometry of the complex **5a** is depicted in Fig. S1 (Supplementary Data). Some of the calculated structural parameters of the Cr(III) complex are listed in Table S1 (Supplementary Data). As can be seen in Fig. S1 (Supporting Information), the ligand **4a** acts as a bidentate ligand and coordinates to the Cr(III) *via* nitrogen atom of the amine functional group and oxygen atom of the carbonyl group. The aromatic rings of the ligand are in a same plane. The other position of the complex is filled by two H_2O molecules. Also, optimized geometry and frequency calculations were done in both of the possible states of the complex, high spin and low spin. The high spin state of the complex is more stable than the low spin state. Their energy difference is 84.23 and 67.12 kJ. Mol^{-1} in the gas phase and PCM model, respectively.

The DFT computed vibrational modes of Cr(III) complex **5a** are listed in Table 1 together with the experimental values for comparison. The atoms are numbered as in Fig. 2. As seen in Table 2, there is good agreement between the experimental and DFT-calculated frequencies of the complex **5a**, confirming validity of the optimized geometry as a proper structure for the complex **5a**.

Based on the optimized geometries and using time-dependent density functional theory (TD-DFT) (Bauernschmitt and Ahlrichs, 1996) methods, the electronic spectrum of the complex **5a** was predicted (Fig. S2, Supplementary Data). The TD-DFT electronic spectra calculations on **5a** show a broad peak at 387 nm (oscillator strength:

Table 1 Selected experimental and calculated IR vibrational frequencies (cm^{-1}) of Cr(III) complex **5a**.

Experimental frequencies	Calculated		
	Frequency	IR Intensity D (10^{-4} esu^2 cm^2)	Vibrational assignment
703 (w)	691	159	υ_{sym}(Cr—N)
714 (w)	725	67	υ_{asym}(Cr—N)
967 (m)	982	210	δ_{op}(C—H) aromatic
1265 (m)	1261	110	υ(C1—N3, C22—N6)
1399 (m)	1406	1732	υ_{asym}(C4—C5—N2) + υ_{asym}(C25—C26—N5)
1451(s)	1413	519	υ(C = C, C=N) of the aromatic rings
	1459	52	υ(C21—C9) + υ(C42—C30)
	1467	310	υ(C=N) of the aromatic rings + υ(C42—N4, C21—N1)
	1473	72	υ(C=N) of the aromatic rings + υ(C22—N6, C1—N3)
1630 (s)	1523	529	υ(C=C) of the aromatic rings
	1564	4123	δ_{sci}(H—O—H) of the H_2O ligands
	1639	321	υ(C=C) of the benzene rings
	1656	45	υ(C=C) of 1 moiety
2822 (m)	3069–3195	25–17	υ_{sym}(C—H) aliphatic
	3082–3119	35–9	υ_{asym}(C—H) aliphatic
	3189–3233	11–9	υ(C—H) aromatic
3375 (vs,br)	3555	45	υ(C28—H21)) + υ(C7—H2)
	3783	19	υ_{sym}(O—H) of the H_2O ligands
	3877	39	υ_{asym} (O—H) of the H_2O ligands

Abbreviation: op, out-of-plane; ip, in-plane; w, weak; m, medium; s, strong; vs, very strong; br, broad; sh, shoulder.

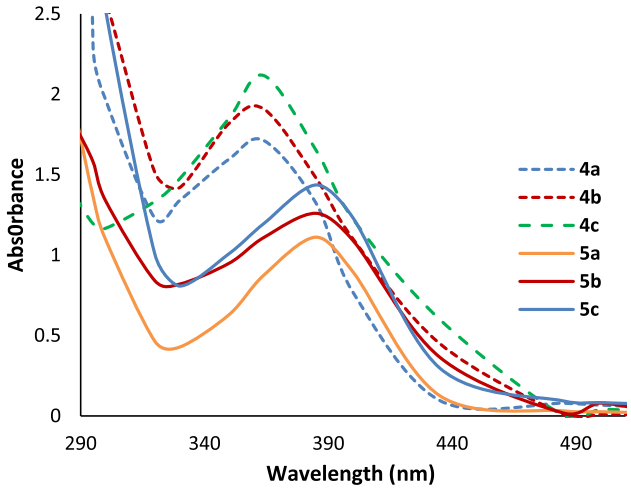

Fig. 2 The absorption spectra of se **4a-c** and Cr(III) complexes **5a-c** in DMSO solution (10^{-4} M).

0.4607), which can be linked to Ligand to-Metal charge transfer (LMCT) (Purwoko and Hadisaputra, 2017) transitions. This electronic transition band can be compared with the experimental value of 395 nm.

3.2. Photophysical properties of the ligands and complexes

UV–Vis and fluorescence spectroscopy in the wavelength range of 200–1000 nm were applied to characterize the absorption and fluorescence emission spectra of fluorescent heterocyclic ligands **4a-c** and Cr (III) complexes **5a-c** (Figs. 2 and 3). Numerical spectral data are also presented in Table 2. Values of extinction coefficient (ε) were calculated as the slope of the plot of absorbance vs concentration. As seen in Fig. 2, the spectra of the complexes **5a-c** have an absorption maximum at 402 nm at which the ligands have no absorbance. An efficient charge transfer of electron from p-orbital on ligand to Cr(III) d-orbital can be considered as the main reason for the color of the complexes explained as Ligand to-Metal charge transfer (LMCT) (Purwoko and Hadisaputra, 2017). Furthermore ligands **4a-c;** and chromium complexes **5a-c** produced fluorescence in dilute solution of DMSO (Fig. 2). The fluorescence quantum yields of the compounds were also determined *via* comparison methods, using fluorescein as a standard sample in 0.1 M NaOH and MeOH solution (Umberger and LaMer, 1945). The used value of the fluorescein emission quantum yield is 0.79 and the obtained emission quantum yields of the new compounds are around 0.66–0.81. As can be seen from Table 2, extinction coefficient (ε) of **4c**, fluorescence intensity and the emission quantum yield in **5b** were the biggest values.

Table 2 Spectroscopic data for **4a-c** and **5a-c** at 298 K.

Dye	4a	4b	4c	5a	5b	5c
λ_{abs} (nm)[a]	360	365	365	395	395	400
$\varepsilon \times 10^{-3}$ [(mol L^{-1})$^{-1}$ cm^{-1}][b]	15.9	18.2	22.2	11.1	12.6	14.4
λ_{flu} (nm)[c]	525	525	525	530	530	530
Φ_F[d]	0.69	0.66	0.73	0.79	0.81	0.80

[a] Wavelengths of maximum absorbance (λ_{abs}).
[b] Extinction coefficient.
[c] Wavelengths of fluorescence emission (λ_{flu}) with excitation at 360 nm.
[d] Fluorescence quantum yield.

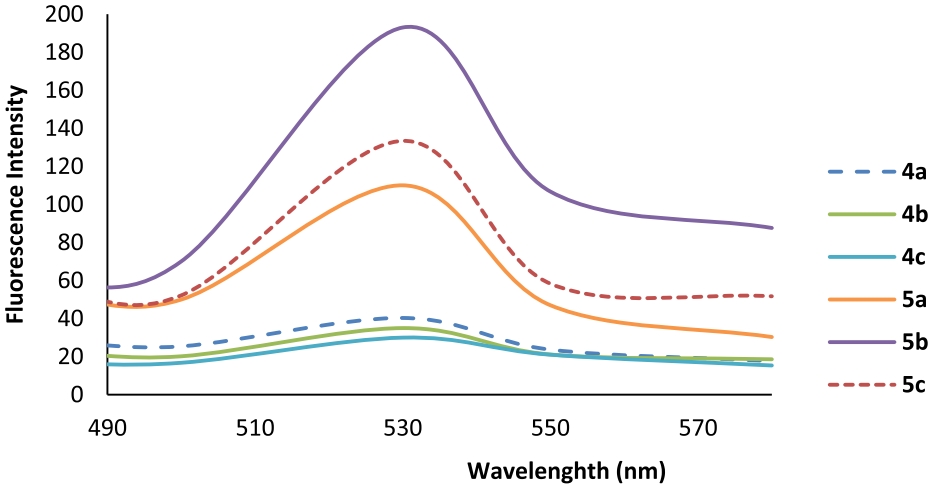

Fig. 3 The fluorescence emission spectra of **4a-c** and Cr(III) complexes **5a-c** in DMSO solution (1×10^{-6} M).

Table 3 Antibacterial activity (MIC, μg mL^{-1}) of reference and compounds **4a-c** and **5a-c.**

Compds.	S.a. (MRSA)	B.s. (ATCC 6633)	P.a. (ATCC 27853)	E.c. (ATCC 25922)
4a	110	95	90	95
4b	95	90	80	80
4c	90	90	80	80
5a	35	30	30	25
5b	25	15	15	15
5c	10	5	10	5
Ampicillin	62	0.50	125	8

3.3. Antibacterial studies

The antibacterial activity of the compounds **4a-c** and **5a-c** was tested against a panel of strains of Gram negative bacterial (*Pseudomonas aeruginosa* (ATCC 27853) and *Escherichia coli*, (ATCC 25922)) and Gram positive (*Methicillin Resistant S. aureus (MRSA)*) clinical isolated and *Bacillus subtilis* (ATCC 6633)) species (Table 3) using broth microdilution method as previously described (Espinel-Ingroff et al., 2015). Comparison with Ampicillin as a standard was done. The lowest concentration of the antibacterial agent that prevents growth of the test organism, as detected by lack of visual turbidity (matching the negative growth control), is designated the minimum inhibitory concentration (MIC). Experimental details of the tests can be found in our earlier study (Pordel et al., 2013).

As can be concluded from Table 3, compounds **4a-c** inhibit the metabolic growth of the tested Gram positive and negative bacteria to the same extent, but the inhibitions percent are less than those of Ampicillin. Coordination of ligands **4a-c** to Cr (III) leads to improvement in the antibacterial activity. This can be explained by Tweedy's chelation theory (Tweedy, 1964), which explicated that the lipophilicity of the uncoordinated ligand can be changed by reducing of the polarizability of the M^{n+} ion *via* the L → M donation, and the possible electron delocalization over the metal complexes. Also, the results revealed that the complex **5c** with R = Bu group, showed greater antibacterial activity against S.a. (MRSA), P.a. (ATCC 27853) and E.c. (ATCC 25922) than did the well known antibacterial agent Ampicillin (Table 3). Considering the selectivity of the action of new compounds, they were applied to normal HDF cells (a category of human skin fibroblasts) and did not show significant toxicity up to 100 mg/l.

4. Conclusion

New fluorescent Cr (III) complexes were obtained from coordination of the ligands derived from benzimidazole with Cr (III) cation. The structures of the ligands and complexes have been established by spectral and analytical data and an octahedral geometry was proposed for the complexes. To gain a deeper insight into geometry and spectral properties of the new complexes, the DFT methods were employed. The DFT-calculated vibrational modes of Cr(III) complexes are in good agreement with the experimental values, confirming suitability of the optimized geometries for the complexes. Fluorescent ligands and chromium complexes were spectrally characterized by UV–Vis and fluorescence spectroscopy. Results revealed that Cr(III) complexes generate fluorescence in dilute solution of DMSO. Also, results from the antimicrobial screening tests revealed that an improvement in the antibacterial activity is observed upon the coordination of the ligands to the Cr(III) ion and the new complexes are more effective against *Pseudomonas aeruginosa* and *Methicillin Resistant S. aureus (MRSA)* species than did Ampicillin. This activity, together with high fluorescence intensity, can offer an opportunity for the study of physiological functions of bacteria such as at single-cell level (Joux and Lebaron, 2000).

Acknowledgment

We would like to express our sincere gratitude to Research Office, Mashhad Branch, Islamic Azad University, Mashhad-Iran, for financial support of this work. We must also acknowledge Maryam Jajarmi (Khorasan Razavi Rural Water and Wastewater Co.) for her assistance in antibacterial studies.

Appendix A. Supplementary material

Supplementary data to this article can be found online at https://doi.org/10.1016/j.arabjc.2019.03.001.

References

Abdel-Rahman, L.H., Abu-Dief, A.M., Aboelez, M.O., Abdel-Mawgoud, A.A., 2017. DNA interaction, antimicrobial, anticancer activities and molecular docking study of some new VO (II), Cr (III), Mn (II) and Ni (II) mononuclear chelates encompassing quaridentate imine ligand. J. Photochem. Photobiol. Biol. 170, 271–285.

Adam, C., Wohlfarth, J., Haußmann, M., Sennefelder, H., Rodin, A., Maler, M., Martin, S., Goebeler, M., Schmidt, M., 2017. Allergy-inducing chromium compounds trigger potent innate immune stimulation via ROS-dependent inflammasome activation. J. Inv. Derm. 137, 367–376.

Bansal, Y., Silakari, O., 2012. The therapeutic journey of benzimidazoles: a review. Bioorg. Med. Chem. 20, 6208–6236.

Bauernschmitt, R., Ahlrichs, R., 1996. Treatment of electronic excitations within the adiabatic approximation of time dependent density functional theory. Chem. Phys. Lett. 256, 454.

Chen, W.Y., Chen, C.J., Lui, C.H., Mao, F.C., 2009. Chromium supplementation enchances insulin signaling in skeletal muscle of obese KK/HIJ diabetic mice. Diabet. Obesity Metabol. 11, 293–303.

Chen, G., Gao, Z., Chu, W., Cao, Z., Li, C., Zhao, H., 2017. Effects of chromium picolinate on fat deposition, activity and genetic expression of lipid metabolism-related enzymes in 21 day old Ross broilers. Asian-Aust. J. Anim. Sci.

Ding, A.J., Wu, G.S., Tang, B., Hong, X., Zhu, M.X., Luo, H.R., 2017. Benzimidazole derivative M084 extends the lifespan of

Caenorhabditis elegans in a DAF-16/FOXO-dependent way. Mol. Cell. Biochem. 426, 101–109.
El-Megharbel, S.M., Refat, M., 2015. Ligational behavior of clioquinol antifungal drug towards Ag (I), Hg (II), Cr (III) and Fe (III) metal ions: synthesis, spectroscopic, thermal, morphological and antimicrobial studies. J. Mol. Struct. 1085, 222–234.
Espinel-Ingroff, A., Chowdhary, A., Gonzalez, G.M., Guinea, J., Hagen, F., Meis, J.F., Thompson, G.R., Turnidge, J., 2015. Multicenter study of isavuconazole MIC distributions and epidemiological cutoff values for the Cryptococcus neoformans-Cryptococcus gattii species complex using the CLSI M27–A3 broth microdilution method. Antimicro. Chemother. 59, 666–668.
Flores-Carrillo, P., Velázquez-López, J., Aguayo-Ortiz, R., Hernandez-Campos, A., Trejo-Soto, P., Yepez-Mulia, L., Castillo, R., 2017. Synthesis, antiprotozoal activity, and chemoinformatic analysis of 2-(methylthio)-1H-benzimidazole-5-carboxamide derivatives: identification of new selective giardicidal and trichomonicidal compounds. Eur. J. Med. Chem.
Frisch, M., Et, A., 2003. Gaussian 03, Revision B.03. Gaussian Inc, Pittsburgh, PA, p. 1101.
Gaba, M., Singh, S., Mohan, C., 2014. Benzimidazole: an emerging scaffold for analgesic and anti-inflammatory agents. Eur. J. Med. Chem. 76, 494–505.
Ghssein, G., Matar, S., 2018. Chelating mechanisms of transition metals by bacterial metallophores ''Pseudopaline and Staphylopine'': a quantum chemical assessment. Computation 6, 56.
Joux, F., Lebaron, P., 2000. Use of fluorescent probes to assess physiological functions of bacteriaat single-cell level. Microbes infect. 2, 1523–1535.
Keller, P., Muller, C., Engelhardt, I., Hiller, E., Lemuth, K., Eickhoff, H., Wiesmuller, K.H., Burger-Kentischer, A., Bracher, F., Rupp, S., 2015. An antifungal benzimidazole derivative inhibits ergosterol biosynthesis and reveals novel sterols. Antimicro. Chem. 59, 6296–6307.
Kumar, A., Kumar, A., Gupta, R., Paitandi, R., Singh, K., Trigun, S., Hundal, M., Pandey, D., 2016. Cationic Ru (II), Rh (III) and Ir (III) complexes containing cyclic π-perimeter and 2-aminophenyl benzimidazole ligands: synthesis, molecular structure, DNA and protein binding, cytotoxicity and anticancer activity. J. Org. Chem. 801, 68–79.
Lee, C., Yang, W., Parr, R.G., 1988. Development of the Colle-Salvetti correlation-energy formula into a functional of the electron density. Phys. Rev. B 37, 785–789.
Liu, B., Chai, J., Feng, S., Yang, B., 2015. Structure, photochemistry and magnetic properties of tetrahydrogenated Schiff base chromium (III) complexes. Spectrochim. Acta Part A: Mol. Biomol. Spect. 140, 437–443.
Liu, Y., Cotillard, A., Vatier, C., Bastard, J.P., Fellahi, S., Stevant, M., Allatif, O., Langlois, C., Bieuvelet, S., Brochot, A., Guilbot, A., 2015. A dietary supplement containing cinnamon, chromium and carnosine decreases fasting plasma glucose and increases lean mass in overweight or obese pre-diabetic subjects: a randomized, placebo-controlled trial. Plos One 10, e0138646.
Mahmoud, W.H., Mohamed, G.G., El-Dessouky, M.M., 2015. Synthesis, structural characterization, in vitro antimicrobial and anticancer activity studies of ternary metal complexes containing glycine amino acid and the anti-inflammatory drug lornoxicam. J. Mol. Struct. 1082, 12–22.
Mandina, Sh., Tawanda, M., 2013. Chromium, 2013. an essential nutrient and pollutant. Afr. J. Pure. Appl. Chem. 30, 310–317.
Pordel, M., Abdollahi, A., Razavi, B., 2013. Synthesis and biological evaluation of novel isoxazolo[4,3-e]indoles as antibacterial agents. Rus. J. Bioorg. Chem. 39, 211–214.
Preston, P.N., 1990. In The Chem. Hetero. Comp. 40, 87–105.
Purwoko, A.A., Hadisaputra, S., 2017. Experimental and theoretical study of the substituted (H6-Arene) Cr (CO) 3 complexes. Orien. J. Chem. 33, 717–724.
Rahimizadeh, M., Pordel, M., Bakavoli, M., Rezaeian, S., Eshghi, H., 2009. Synthesis of a new heterocyclic system—Fluoreno[1,2-*d*] imidazol-10-one. Can. J. Chem. 87, 724–728.
Saini, S., Dhiman, N., Mittal, A., Kumar, G., 2016. Synthesis and antioxidant activity of the 2-methyl benzimidazole. J. Drug Del. Thera. 6, 100–102.
Sarin, V., Sarvinder Singh, T., Pant, K.K., 2006. Thermodynamic and breakthrough column studies for the selective sorption of chromium from industrial effluent on activated eucalyptus bark. Bioresour. Techonol. 97, 1986–1993.
Siddiqui, N., Alam, M.S., Ali, R., Yar, M.S., Alam, O., 2016. Synthesis of new benzimidazole and phenylhydrazinecarbothiomide hybrids and their anticonvulsant activity. Med. Chem. Res. 25, 1390–1402.
Siddiqui, N., Alam, M., Sahu, M., Yar, M., Alam, O., Siddiqui, M., 2016. Antidepressant, analgesic activity and SAR studies of substituted benzimidazoles. As. J. Pharm. Res. 6, 170–174.
Tomasi, J., Cammi, R., 1995. Remarks on the use of the apparent surface charges (ASC) methods in solvation problems: Iterative versus matrix-inversion procedures and the renormalization of the apparent charges. J. Comput. Chem. 16, 1449.
Tweedy, B., 1964. Plant extracts with metal ions as potential antimicrobial agents. Phytopathology 55, 910–914.
Umberger, J.Q., LaMer, V.K., 1945. The kinetics of diffusion controlled molecular and ionic reactions in solution as determined by measurements of the quenching of fluorescence. J. Am. Chem. 67, 1099.
Van Oosten, M.J., Silletti, S., Guida, G., Cirillo, V., Di Stasio, E., Carillo, P., Woodrow, P., Maggio, A., Raimondi, G., 2017. A benzimidazole proton pump inhibitor increases growth and tolerance to salt stress in Tomato. Front. Plant. Sci. 2017, 8.
Vausselin, T., Seron, K., Lavie, M., Mesalam, A.A., Lemasson, M., Belouzard, S., Feneant, L., Danneels, A., Rouille, Y., Cocquerel, L., Foquet, L., 2016. Identification of a new benzimidazole derivative as an antiviral against hepatitis C virus. J. Virol. 90, 8422–8434.
Vosburgh, W.C., Chromium, G., 1941. Complex ions. I. The identification of complex ions in solution by spectrophotometric measurements. J. Am. Chem. 63, 437.
Whitfield, P., Parry-Strong, A., Walsh, E., Weatherall, M., Krebs, J., 2016. The effect of a, loss and lipid parameters in type 2 diabetes: an open-label cross-over randomised controlled trial. Eur. J. nut. 55, 1123–1131.
Yang, H., Ren, Y., Gao, X., Gao, Y., 2016. Synthesis and anticoagulant bioactivity evaluation of 1,2,5-trisubstituted benzimidazole fluorinated derivatives. Chem. Res. Chin. Univ. 32, 973–978.
Yousefi, Z., Eshtiagh-Hosseini, H., Salimi, A., Janiak, A., 2015. Exploring the influence of crystal environment on the geometry of bis(pyridine-2,6-dicarboxylato) chromium (III) anionic complexes containing various cationic moieties: synthesis, structures and Hirshfeld surface analysis. J. Mol. Struc. 1083, 460–470.
Zhang, Y., Xu, J., Li, Y., Yao, H., Wu, X., 2015. Design, synthesis and pharmacological evaluation of novel NO-releasing benzimidazole hybrids as potential antihypertensive candidate. Chem. Bio. D. Des. 85, 541–548.
Zhou, W., Yu, T., Vazin, M., Ding, J., Liu, J., 2016. Binding to DNA backbone phosphate and bases: slow ligand exchange rates and metal hydrolysis. J. Inorg. Chem. 55, 8193–8200.
Ziegenfuss, T.N., Lopez, H.L., Kedia, A., Habowski, S.M., Sandrock, J.E., Raub, B., Kerksick, C.M., Ferrando, A., 2017. Effects of an amylopectin and chromium complex on the anabolic response to a suboptimal dose of whey protein. J. Inter. Soc. Sp. Nut. 14, 6.